ASSESSMENT OF CLADDING MATERIALS CORROSION BEHAVIOR FOR SCW-SMR IN STATIC CONDITIONS: RESULTS OBTAINED IN ECC SMART PROJECT

MANUELA FULGER, DANIEL PETRESCU, VALENTIN LĂUTARU, AUREL DAVID, and CĂTĂLIN MARIAN DUCU

[1)] Corrosion Dept., Institute for Nuclear Research (RATEN ICN) Pitești, Romania
[2)] RATEN, Romania
e-mail: manuela.fulger@nuclear.ro

Abstract

Supercritical water (SCW) systems, as proposed GenIV concept, aim to increase efficiency by ~45% compared to current light water reactors. Despite the obvious benefits of supercritical water-cooled technology, there are still technological challenges, one of the most important being the selection of fuel cladding materials that can withstand the harsh conditions of supercritical water (SCW), particularly at high temperatures and pressures. After more than two decades of research, the list of potential structural materials for SCWRs has been gradually reduced to a few candidates, including austenitic steels, advanced ferritic-austenitic (AFA) alloys, and oxide dispersion-strengthened (ODS) alloys. The European ECC SMART (Joint European Canadian Chinese Development of Small Modular Reactor Technology) project aimed to focus on developing a pre-design of a SCW-SMR, which also included long-term testing of candidate materials for fuel cladding. Within the framework of ECC SMART project, the Work Package 2 (WP2) conducted studies to assess the effect of the environment at different temperatures and pressures on the selected materials, the effect of tubes' geometry, the effect of neutron radiation, as well as studies of radiolysis in SCW. This paper presents recent findings from static corrosion tests performed by RATEN ICN, as a partner in WP2 of the ECC SMART project. The tests were carried out up to 7000 hours in supercritical conditions on two candidate materials (310S stainless steel and 800H alloy) highlighting their performance and degradation behavior in a highly corrosive SCW environment.

Keywords: *Chromium content, Alloy 800H, Stainless steel 310S, Static conditions*

Introduction

The supercritical water-cooled reactor (SCWR) is one of the six most promising concepts identified by the Generation IV International Forum (GIF) [1]. SCWRs, as a GEN IV concept, are intended to operate with water at higher temperatures and pressures than GEN III reactors, to increase the plant's thermodynamic efficiency, resulting in more electricity for the same amount of fuel.

After a long period of focus on large nuclear power plants development, there is an increased interest in small and modular reactors (SMRs) for electricity generation, heat generation, cogeneration and desalination. Several SMR technologies that align with most of the GEN IV concepts are now being globally developed. As interest in SMR technology has grown, SCWR concept configuration has been scaled down to assess the feasibility of a supercritical water-cooled small modular reactor (SCW-SMR) having both the advantages of a SCWR and an SMR. SMRs offer savings in cost and construction time, and they can be deployed incrementally to match increasing energy demand [2]. SCW-SMR technology can replace ~300 MWe fossil-fired plants, potentially reducing the construction costs.

Understanding the high-temperature corrosion of steels operating at high temperatures is critical to ensuring the power equipment durability [3]. SCWR' high temperature and pressure operating conditions, as well as their high neutron flux and long operating time, require materials that are mechanically and corrosion resistant, and have reliable lifetime. Currently, some of the main candidate materials, recommended for use in the SCWR core, are widely available materials, such as Alloy 800H and 310S stainless steel [4].

The aim of the H2020 ECC SMART project was to provide the design requirements for the future SCW-SMR technology and to develop the pre-licensing study to prove safety in later stages of SCW-SMR concept development [5]. In order to support the SCW-SMR construction materials qualification process, WP2, the largest of the project's six work packages, is focused on materials testing, aiming to understand the corrosion behaviour of some candidate materials under various conditions. In order to simulate the real conditions and support progress in the field of SCW-SMR, a stainless steel (SS 310S) and an austenitic alloy (Alloy 800H) were selected to be tested in the shape of semi-tubes, being aware that in the case of fuel cladding the SCW will only wet the outer surface of the tube.

This paper presents the most important findings from long-term oxidation tests conducted under static conditions at 500ºC and 25MPa.

Experimental work

The materials for corrosion testing were procured from UNIONCEL (Czech Republic), machined at CVR and distributed to all partners in WP2.The shape of specimens was chosen because it possesses concave and convex surfaces, which can exert different stresses on the oxide layer with important implications on the surface of fuel cladding.

The semicylindrical specimens cut from SS 310S and 800H alloy chemical composition (according to the producer's certificate) is summarized in Table 1.

Table 1. Chemical composition (in %wt) of material specimens according to producer's certificates

Element %wt Alloys	C	Si	Mn	P	S	Ni	Cr	Cu	Ti	Al	Mo	Co	Fe
310S	0.06	0.39	1.190	0.024	0.0006	21.45	**25.27**	-	-	-	0.25	-	Bal
800H	0.08	0.2	0.7	≤ 0.03	0.0005	30.7	**19.7**	0.45	0.58	0.4	0.18	0.11	Bal

The SCW exposure tests were conducted in demineralized water at 500 °C, and 25 MPa, for 1000 h, 2000 h, and 4000 h, respectively, using static autoclaves, according to the specified exposure conditions (demineralized water, 150 ppb of dissolved oxygen).

The chosen temperature and pressure (500 °C / 25MPa) represent the SCW-SMR expected operating conditions. After each exposure period, three specimens from every material were removed from autoclaves and subjected to gravimetric and metallographic analysis. Specimens were mounted on pre-oxidized 316L wires fixed to a pre-oxidized rack. It is important to note that static autoclaves provide less control over water chemistry - such as dissolved corrosion products and anionic impurities - compared to loop circuits, due to the sealed nature of the vessel. Each specimen was weighed 5 times, before and after each exposure in SCW, using a Kern analytical balance with an accuracy of ± 0.01 mg. The differences represent the weight change during the exposure in SCW. To characterize the specimens after oxidation, several different analysis methods such as optical microscopy and SEM/EDS analysis were used.

Oxide layers morphology was analyzed using a Scanning Electron Microscope (SEM) TESCAN LMU equipped with a field emission gun. To analyze the microstructure of the specimens a light optical microscope Olympus GX 71 (equipped with lenses with a long working distance and a magnification from 12.5 x up to 2000x) was used.

Microhardness measurements were performed using an OPL microhardness tester operating in automatic mode with a 100 g load (MHV 0.1). The upper parts (~5 mm) of the analysed specimens were sectioned and individually embedded in conductive copper resin.

Results obtained

Gravimetric analysis

Figure 1 shows a comparison of the average mass changes calculated for the specimens oxidized for different periods.

After oxidation in water at 500 °C and 25 MPa, the two types of specimens exhibit distinct mass gain behaviour (see Fig. 1). The 800H alloy has a significantly higher oxidation rate than the SS 310S, with a mass gain that is about five times greater after 7000 hours of exposure.

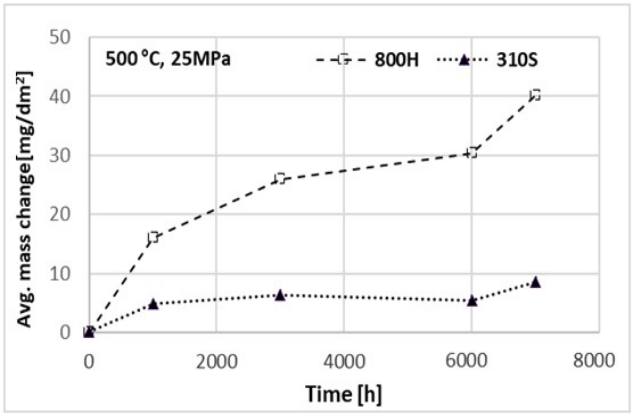


Fig. 1. Average mass change of SS 310S and Alloy 800H as a function of exposure time in water at 500°C, 25 MPa

The lower weight gain observed in SS 310S is attributed to its higher chromium content, which promotes thinner oxide layers formation. To investigate this, morphological analyses of the oxide layers and measurements of their thickness were performed. Samples exposed for 6000 hours were excluded from further SEM/EDS analysis and were only subjected to gravimetric measurements, so oxide layer spallation - which could explain the observed mass decrease in SS 310S - cannot be confirmed.

It is considered that oxides developed on the cladding surfaces can modify the thickness of tubes, influencing the structural integrity and mechanical properties of the material, leading to failure during operation.

To estimate fuel cladding corrosion, the weight gain can be converted into penetration depth to indicate the metal loss during oxidation. This can be calculated using David Guzonas's theoretical Equation, and assuming that entire oxidized metal ions are retained on the surface (no spalling or oxide dissolution).

$$Penetration\,depth[\mu m] = WG\left[mg/dm^2\right] \times \left(\frac{1-f_{o/ox}}{f_{o/ox}}\right)\frac{1}{\rho_{alloy}}$$

where WG is the weight gain, $f_{o/ox}$ (0.276) is the weight fraction of oxygen in the magnetite (which was assumed to be the major oxide) and ρ is the density of the alloy (a density of 8.03 g/cm^3 for alloy 800H, and of 7.9 g/cm^3 for SS 310S, respectively, was considered).

Since the designed lifetime of the SCW-SMR is estimated to be approximately 3 to 5 years, the wall penetration was calculated after the maximum operating period of SMRs (~30000h) and is presented in Table 2.

According to references [6] and [13], maximum allowable corrosion penetration for Canadian SCWR fuel cladding is 200 µm after 30,000 hours of operation, while that for High-Performance Light Water Reactor (HPLWR) fuel cladding is 140 µm after 20,000 hours of operation.

Table 2. Penetration depth calculated for both alloys exposed in SCW at 500 ºC /25MPa

Parameters	**Value**							
Temperature [^{0}C]	500				500			
Presssure [MPa]	25				25			
Alloys	800H				310S			
Density [g/cm^3]	8.03				7.90			
Test duration [h]	1000	3000	6000	7000	1000	3000	6000	7000
Weight gain (WG) [mg/dm^2]	16.06	25.9	30.9	40.14	4.79	6.39	5.46	8.61
Penetration depth [µm]	0.50	0.89	1.06	1.40	0.16	0.20	0.19	0.30
Penetration rate [µm/y]	4.80	2.60	1.50	1.70	1.46	0.65	0.27	0.37
Wall penetration depth after 30,000 hours [µm]	16.5	8.90	5.30	5.90	5.02	2.2	1.00	1.28

For both selected materials, the estimated wall penetration after 30,000 hours remains below 20 µm, even considering the highest penetration rate values (obtained after 1,000 hours), as can be seen in Table 2. Given the information from the literature mentioned above, it is unlikely that oxide formation during this period will compromise structural integrity of both alloys.

Oxide morphology analysis

The oxidized specimens were examined by SEM after various times of exposure to SCW, in order to identify the morphologies of oxide layers formed on the alloy surfaces. Figure 2 presents the aspects of oxides after the longest time of oxidation (7,000 h) at 500 ºC/ 25MPa. The images correspond to internal and external side of the specimens.

It can be observed a difference between the internal and external sides of both types of specimens.

In case of alloy 800H, on the inner side a dense layer with polyhedral, larger oxides crystals aglomerated on a layer with smaller oxides can be observed, while on the external side the image reveals a dense cover of smaller and rounded crystals homogeneously distributed.

In case of SS 310S, on the inner side, larger, polyhedral and rare oxide crystals developed on an internal oxide layer can be observed, while on the outer side of the same specimen, islands of larger oxide crystals with elongated shape have developed.

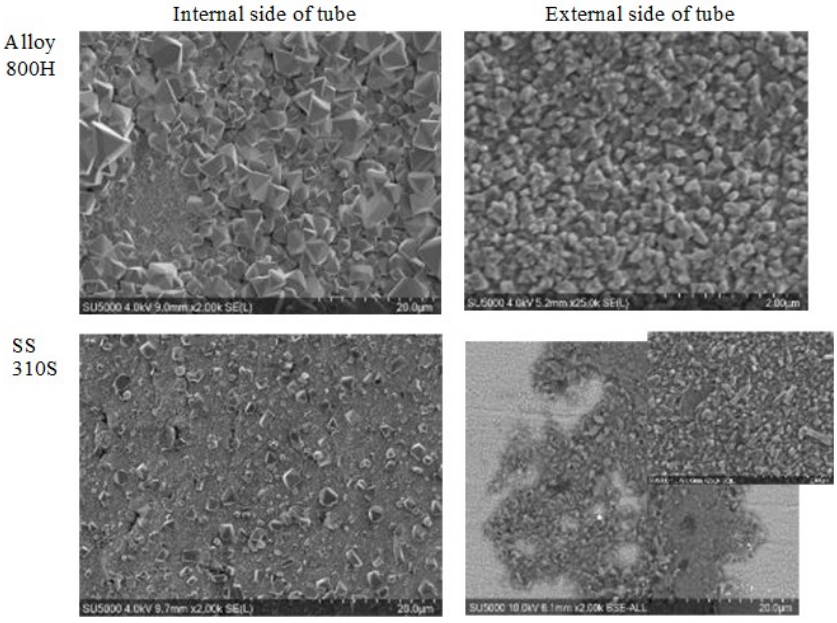


Fig. 2. SEM images of oxides formed on both alloys at 500 °C/ 25 MPa after 7,000 h on the internal and external sides of the tubes

Oxide layers thickness

Oxide thicknesses were measured in cross-section, after embedding in the resin, using an optical microscope.

Figure 3 presents the oxide thicknesses measured on the samples tested at 500 °C/ 25MPa. The thickness values are seen under each optical micrograph in the figure.

A thickening of the oxide developed on these candidate materials would have implications for heat transfer. The oxides developed at 500 °C had greater thicknesses on the internal surface of the tubes compared to the external surface. In the case of cladding materials the relevant surface is the outer one.

Thus, analyzing only the oxides formed on the outer surface, it was observed that after the longest oxidation period (7,000 h) at 500 °C / 25MPa, the oxides are thin, the thickness values falling within the allowed limits. According to the optical microscopy measurements, the oxides formed after 7,000 hours on the outer surface of the SS 310S tube had thicknesses of maximum 1.51 µm, while those formed on the outer surface of alloy 800H had thicknesses of maximum 1.77 µm.

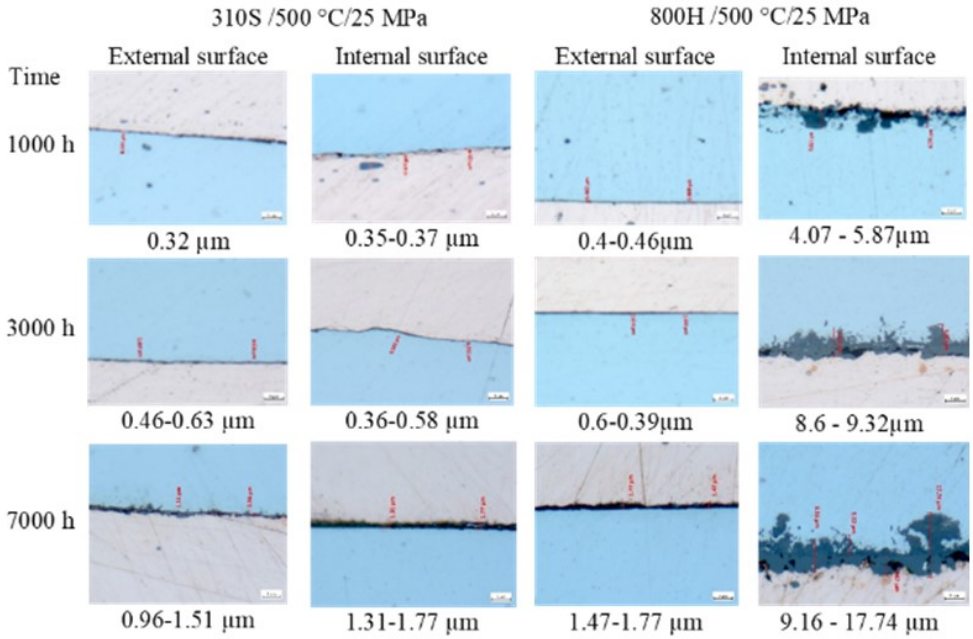


Fig. 3. Optical microscopy images: oxide thicknesses measurements on specimens at 500 °C/25 MPa up to 7,000 h

On the internal surface of the 800H tubes it was observed a "mixed" oxide (composed of an external oxide and an internal oxide that penetrated the material). This oxidation was considered as an internal oxidation phenomenon. Internal oxidation is a kind of selective oxidation in which oxygen diffuses into the bulk metal and reacts with the more reactive alloying elements causing sub-surface precipitation of the alloying element oxides and in time can lead to the intergranular cracking of the alloy [10].

The internal oxidation zones were observed on the Alloy 800H specimens starting from 1,000 h of oxidation (see Fig. 4) and seem to occur in the areas where from the beginning, on the as-received samples, secondary phases of Cr, Ti carbides or nitrides existed. Because the carbides are located close to the surface, the thermodynamics of the oxidation reaction at high temperature and pressure favored their oxidation by the inward diffusion of oxygen.

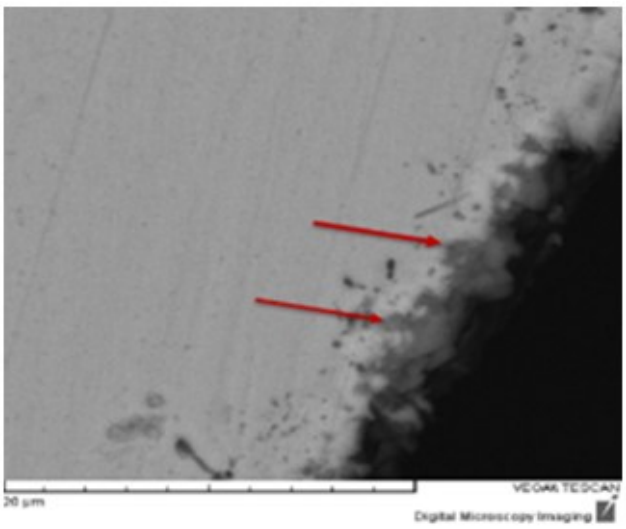


Fig. 4. SEM image- inner side microstructure on alloy 800H tube after 1,000 h at 500 °C /25 MPa

Microstructural analysis of specimens after oxidation

During long-term exposure to SCW at high temperature, the alloys' microstructure can undergo changes, so the specimens were analysed from a microstructural point of view. In Fig. 5, the specimens' microstructure is presented, after oxidation for 7,000 h in water at 500 °C/25 MPa.

In case of oxidized alloy 800H specimens, a decrease in the grain size and a reduction in the number of the twin grains was observed as the temperature and oxidation time increase, which can be explained by a recrystallization of the grains during oxidation.

After 7,000 h at 500 °C/25 MPa, at higher magnification, the SS 310S specimens exhibit coarse grain boundaries (see Fig. 5d) in comparison with the alloy 800H specimen. This type of grain boundaries may correspond to the formation of Cr-rich carbides and the concomitant development of Cr-depleted zones, which can lead to "sensitization" of the microstructure and increased susceptibility to intergranular corrosion [11]. Similar to formation of the M23C6 carbide precipitate, the formation of the σ-phase precipitate can also be accompanied by an adjacent Cr-depleted zone formation, which also can increase the susceptibility to intergranular attack. The time at which a σ-phase begins to nucleate depends on the presence of M23C6 carbide particles not dissolved during solution treatment.

Optical micrographs of the 310S specimens exposed for 7000h at 500 °C/25 MPa are shown in Fig. 6. In these images, the presence of precipitated carbides at the grain boundaries and also the presence of the sigma phase are highlighted. To highlight the sigma phase, two types of electrolytic etching were used: one with a 10% oxalic acid solution and another with a 10% ammonium persulfate solution [12]. The observed microstructural changes are complemented by information from the measurements showing an increase in microhardness values with increasing oxidation time and temperature.

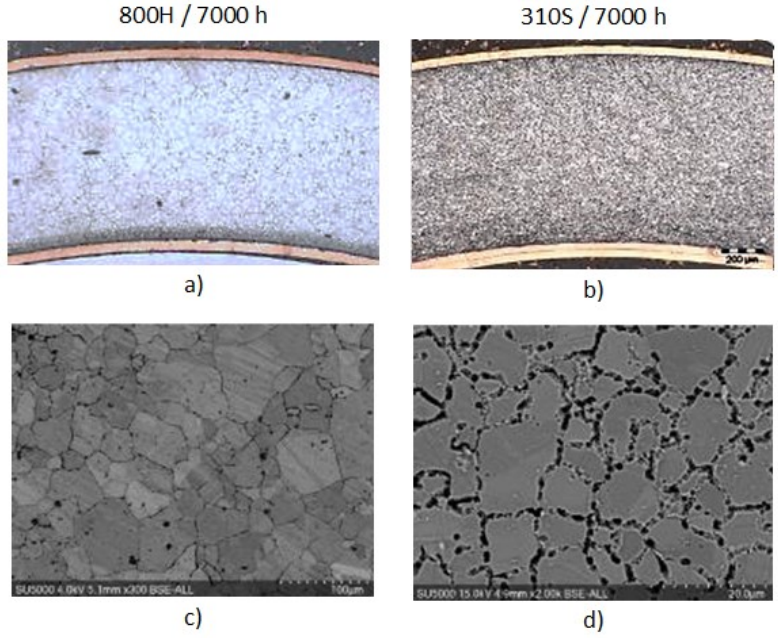


Fig. 5. Microstructure of specimens oxidized in water at 500 °C / 25 MPa for 7,000 h
a) alloy 800H (OM); b) SS 310S (OM); c) alloy 800H (SEM); d) SS 310S (SEM)

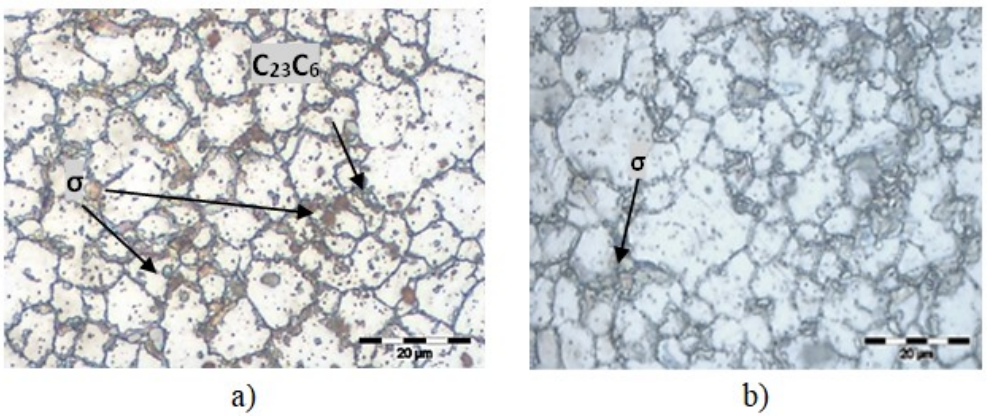


Fig.6. Optical micrographs of the SS 310S specimens exposed in water at 500 °C/25 MPa, for:
a) 7000h (etched with oxalic acid 10%), b) 7000 h (etched with ammonium persulfate 10%)

The Vickers microhardness (MHV0.1) was measured in cross section on as-received and oxidized samples (Fig 7).

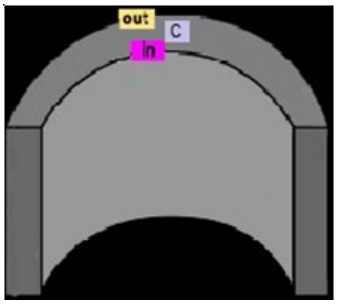


Fig. 7. Cross section zone used for microhardness measurement

The values from Table 3 were obtained by averaging three measurements on a single sample of each type of alloy.

Figure 8 presents the evolution of microhardness values after different times of exposure in water at 500 °C, and 25MPa.

SS 310S samples showed higher microhardness values in as-received state, probably because they were subjected to cold working during manufacturing.

In water at 500 °C/25 MPa, microhardness values tend to increase with oxidation time, the highest values being found after 7000 h for both types of samples in the areas close to the inner and outer diameter of the tubes. In case of SS 310S, after 7000 h, it was a slight decrease in microhardness observed in the center of the sample. An explanation can be the presence of carbides that, through precipitation, induce a softening of the matrix due to chromium depletion.

Table 3. Microhardness values for Alloy 800H and SS 310S (MHV 0.1)

Samples	Condition	OD *	C *	ID *
800H tube	as-received	179.58	157.46	157.33
		500 °C / 25MPa		
	1000h	206.6	195.8	208.9
	3000h	233.9	193.26	192.08
	7000h	251.31	214.69	238.59
310S tube	as-received	289.22	248.31	254.19
		500 °C / 25MPa		
	1000h	310.98	294.8	298.94
	3000h	324.48	317.6	345.62
	7000h	366.6	306.86	392.24

* OD = outer diameter; C = center; ID = inner diameter

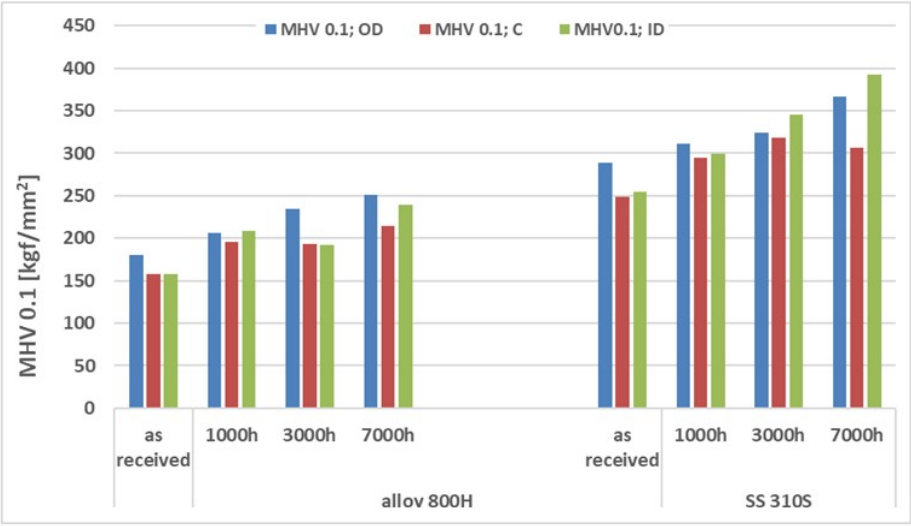


Fig. 8. Vickers microhardness values measured on specimens at 5000 C and 25Mpa, after different periods of oxidation

Conclusions

Oxidation tests have been performed in static autoclaves. After oxidation in water at 500 °C and 25 MPa, clear differences appeared between the analysed alloys, Alloy 800H specimens showing a higher oxidation tendency than SS 310S (a mass gain almost 5 times higher than 310S).

From the point of view of wall penetration, calculations showed that after 30,000 hours of oxidation, penetration depth is below 20 µm for both alloys, falling within the permitted limits.

After the longest oxidation period considered (7000 h) at 500°C and 25 MPa, the oxides formed on the outer surface of both types of alloys are thin, and the thickness values are within the allowed limits.

In the case of 800H specimens, areas of internal oxidation were observed after 1000 hours of oxidation in water at 500°C and 25MPa, which raises questions regarding susceptibility to intergranular corrosion.

SS 310S samples did not show internal oxidation until after 7000 hours in water at 500°C and 25MPa, but they developed sigma phases and carbides at the grain boundaries, which raises the issue of material sensitization.

Microhardness values show a trend of increasing with oxidation time and temperature for both alloys tested, especially for alloy 310S in the areas where carbides develop.

ACKNOWLEDGEMENTS

The project which includes the results presented and discussed in this paper has received funding from the Euratom research and training programme 2019-2020, under grant agreement No 945234, ECC SMART.

References

[1] Schulenberg, T., Leung, L.K.H., Brady, D., Oka, Y., Yamada, K., Bae, Y., Willermoz, G. (2021) ″Supercritical Water-Cooled Reactor (SCWR) Development through GIF Collaboration″, paper ID IAEA-CN-164-5S06, *Proc. of Int. Conf. on Opportunities and Challenges for Water Cooled Reactors in the 21 Century*, IAEA book, ISBN 978-92-0-164210-3.

[2] Zang, J., Huang, Y. (2021) ″Supercritical Water-Cooled Small Modular Reactor R&D″, *J. of Nucl. Power Engineering,* vol. 42(6), pp. 72-76, doi: 10.13832/j.jnpe.2021.06.0072.

[3] Gwoździk, M., Bramowicz, M., Kulesza, S. (2020) ″Surface morphology analysis of oxide layers formed on 10CrMo9-10 steel used in the power industry″, *Mater. Res. Express*, vol. 7 (2), doi:10.1088/2053-1591/ab5ea9.

[4] Edwards, M., Rousseau, S., Novotný, R., Gong, B., Fulger, M., Penttilä, S., Toivonen, A., Sàez-Maderuelo, A., Zhang, L., Guzonas, D., Huang, X. (2022) ″The reproducibility of corrosion testing in supercritical water - Results of a second international interlaboratory comparison exercise″, *J. of Nuclear Materials*, vol. 565, paper no. 153759, https://doi.org/10.1016/j,jnucmat.2022.153759 .

[5] Marusakova, D., Sipova, M. (2022) ″Material research for small modular reactor cooled by supercritical water – ECC-SMART″, Proc. of conf. METAL 2022, paper no 4480.

[6] Guzonas, D.A., Edwards, M.E., Zheng, W. (2016) ″Assessment of Candidate Fuel Cladding Alloys for the Canadian Supercritical Water-cooled Reactor Concept″, *J. Nucl. Eng. and Rad. Sci.*, vol. 2, paper no. 011016.

[7] American Society of Mechanical Engineers (2020) *″ASME Boiler and Pressure Vessel Code: Section III, Division 1, Subsection NH - Rules for Construction of Nuclear Facility Components: Class 1 Components in Elevated Temperature Service″*, ASME Int., USA.

[8] ASTM INTERNATIONAL (2023) *″Standard Test Methods for Determining Average Grain Size″*, ASTM E112 -13.

[9] Berthod, P. (2007) ″Influence of Chromium Carbides on the High Temperature Oxidation Behavior and on Chromium Diffusion in Nickel-Base Alloys″, *Oxid. Met.*, vol. 68(1–2), pp. 77–96.

[10] Chen, K., Zhang, L., Wu, S., Shen, Z. (2021) ″High-resolution characterization of the internal and external oxidation of austenitic alloys in supercritical water″, *Scripta Materialia*, vol. 197, paper 113814, https://doi.org/10.1016/j.scriptamat.2021.13814.

[11] Hsieh, C.C., Wu, W. (2012) ″Overview of Intermetallic Sigma (σ) phase precipitation in Stainless Steels″, *ISRN Metallurgy*, vol. 2012, paper ID 732471, 16 pgs., doi:10.5402/2012/732471.

[12] Barcik, J. (1988) ″Mechanism of σ-phase precipitation in Cr-Ni austenitic steels″, *Mat. Sci. and Tech.*, vol. 4(1), pp. 5-15.

[13] INTERNATIONAL ATOMIC ENERGY AGENCY (2019) ″Status of Research and Technology Development for Supercritical Water Cooled Reactors″, IAEA TECDOC-1869, IAEA.

[14] Akhiani, H., NezaKat, M., Penttila, S., Spuznar, J. (2016) ″Microstructural Effects on the Oxidation Behavior of Alloy 800HT in supercritical water″, *J. of Nucl. Eng. and Rad. Sci.*, vol. 2, paper no. 021009-1.

[15] Schwind, M., Kallqvist, J., Nilsson, J-O., Agren, J., Andren, H-O. (2000) ″σ-phase precipitation in stabilized austenitic stainless steels″, *Acta Materialia*, vol. 48, pp. 2473-2481.

[16] Vander Voort, G.F. (1984) *″Metallography: Principles and Practice″*, McGraw-Hill Book Co., reprinted by ASM International.